NJC

PAPER

View Article Online
View Journal | View Issue

Cite this: *New J. Chem.*, 2016, **40**, 8060

How does the chain length of PEG functionalized at the outer surface of mesoporous silica nanoparticles alter the uptake of molecules?

Leandro C. Fonseca,*[a] Amauri J. de Paula,[b] Diego Stéfani T. Martinez[c] and Oswaldo L. Alves*[a]

Received (in Montpellier, France) 25th April 2016,
Accepted 28th July 2016

DOI: 10.1039/c6nj01316c

www.rsc.org/njc

The current work describes the development of new mesoporous silica nanoparticles (MSNs) containing a high content of phenyl groups (hydrophobic species) inside the mesopores and externally functionalized with polyethylene glycol (PEG), a hydrophilic moiety, to provide biocompatibility and colloidal stability. The MSNs were encapsulated with curcumin, a versatile hydrophobic drug for biological use. The ability of silica nanoparticles to optimize the solubility of this biologically-active molecule in water was investigated. Nanoparticles were characterized using ^{13}C and ^{29}Si Nuclear Magnetic Resonance (NMR), thermal analysis (TGA and DTA), nitrogen sorption analysis, transmission electron microscopy (TEM), dynamic light scattering (DLS) and zeta potential (PZ). We assessed the curcumin water solubility using the pegylated nanoparticles as well as the influence of the PEG chain length (500 and 2000 Da) and its concentration on the encapsulation process. The results indicate that the higher the PEG chain length the lower the MSN encapsulation capacity for curcumin, possibly due to steric factors. However, all of the nanoparticles largely improved curcumin solubility in water.

Introduction

Wu *et al.*[1] reported silica porous nanoparticles (NPs) containing polyethylene glycol (PEG) conjugated to folic acid on the external surface and internal pores with hematite as the magnetic core for selective application in antitumor treatment. On the other hand, Hu *et al.*[2] designed silica porous nanoparticles consisting of PEG on the outer surface and the inner surface (*i.e.* the interior of pores) with no functional hydrophobic species, to evaluate the influence of this polymer on the hemolysis of Red Blood Cells (RBCs). Finally, Tail *et al.*[3] reported silica nanoparticles with an inner surface functionalized with hydrophobic groups, an outer surface that is free of polyethylene glycol, and the NPs were incorporated with hydrophobic anticancer drugs within their pores, which prevented premature release prior to reaching the target cell during circulation in blood.

These mentioned studies describe pegylated silica nanoparticles that are either free of hydrophobic functionalizing species on the inner surface or nanocarriers with the same chemical nature consisting of phenyl groups on the inner surface but no functionalized PEG on the outer surface. However, there have been no reports on mesoporous silica nanoparticles simultaneously containing both PEG (on the outer surface) and phenyl groups (inside the pores), which might provide synergistic interactions resulting in high colloidal stability, biocompatibility and lower toxicity due to the presence of the polymer, as well as a significant drug loading capacity due to the presence of the aromatic function.

The primary challenge associated with the clinical use of antitumor drugs is the side effects due to their low selectivity for cellular action (resulting in damage to healthy cells in the body), requiring high doses to ensure an effect on the target cells.[4–7] Major antitumor agents that have been used in chemotherapy include camptothecin, cisplatin and 5-fluorouracil to treat lung cancer,[8] and annamycin, doxorubicin and lurtotecan for the treatment of tumor cells in kidneys (carcinoma) and the stomach.[9] Another potential hydrophobic drug is curcumin, which has several medical uses, including antitumor, anti-inflammatory, anti-oxidant, antiseptic and anti-malarial applications.[10–12] Curcumin, which is extracted from the *Curcuma longa* herb, has natural antitumor activity and versatile medical applications.[12] However, differently from hydrophilic drugs, the curcumin

[a] *Laboratory of Solid State Chemistry, Institute of Chemistry, Universidade Estadual de Campinas (UNICAMP), Campinas, São Paulo 13083-970, Brazil. E-mail: leandro.fonseca89@gmail.com, oalves@iqm.unicamp.br; Fax: +55 19 3521 3029; Tel: +55 19 3521 3394*

[b] *Solid-Biological Interface Group (SolBIN), Department of Physics, Universidade Federal do Ceará (UFC), Campus do Pici, Fortaleza, Ceará 60455-900, Brazil*

[c] *Brazilian Nanotechnology National Laboratory (LNNano), Brazilian Center for Research in Energy and Materials (CNPEM), Campinas, São Paulo 13083-970, Brazil*

insolubility in water prevents its efficient use without conjugating it with other elements. Consequently, there is a need to develop molecular vehicles with properties that increase the water solubility of the drug, prevent its capture by the immune system, prolong its blood circulation, improve its efficacy and its lower toxicity.

Therefore, we sought to develop new mesoporous silica nanoparticles consisting of PEG on the outer surface and functionalized mesopores with a high content of phenyl groups (hydrophobic species) in order to create a favorable environment for hydrophobic drugs. We used silica nanoparticles in the study because they are considered to be potential carriers of anticancer drugs owing to an extensive surface area (>900 m^2 g^{-1}), a high pore volume (>0.9 cm^3 g^{-1}) and a wide distribution range of pores (2–10 nm), properties that make them effective in drug delivery applications.[13–16] In addition, these nanoparticles have biocompatibility, and the silanol groups on their surfaces allow a variety of functionalization strategies that provide new chemical properties.[17–20] Because of its natural origins and multiple medical applications, curcumin was chosen as the model drug for encapsulation in silica nanoparticles for the preparation of versatile nanoparticles.

The synthetic strategy involved the functionalization of the external surface of silica nanoparticles using methoxy-PEG 500 Da ($mPEG_{500}$) at the functionalization rates of 10 and 50% mol-Si and methoxy-PEG 2000 Da ($mPEG_{2000}$) at the functionalization rate of 10% mol-Si%. In addition, the inner surface was functionalized with a high content of phenyl groups (30% mol-Si; *i.e.*, with 30% mol-Si of phenyltriethoxysilane). After synthesis, we assessed the ability of the silica nanoparticles to optimize the water solubility of curcumin and the influence of the amount and weight (size) of PEG on the encapsulation process.

Experimental

Materials

Phenyltriethoxysilane (PTES, 98.0%) and tetraethylorthosilicate (TEOS, 98.0%) were purchased from Acros Organics. Cetyltrimethylammonium bromide (CTAB, $\geq$98.0%) and (3-glycidoxypropyl)trimethoxysilane (silane GPS, $\geq$98.0%) were purchased from Sigma-Aldrich Co. LLC. 2-[Methoxy(polyethyleneoxy)6-9propyl]trimethoxysilane (500 Da, silane PEG_{500}, 90.0%) was purchased from Gelest Inc. Potassium hydroxide (KOH, $>$85.0%) was purchased from Vetec. mPEG–COOH 2000 Da (PEG_{2000}, $>$95.0%) was purchased from Nanocs Inc. Ammonium hydroxide (NH_4OH, 27.0%), hydrochloric acid (HCl, 36.5–38.0%) and absolute ethanol (EtOH, $>$95.0%) were purchased from Synth.

Synthesis of MSNs with internal phenyl groups (NP–SiOH)

The synthesis of nanoparticles with internal phenyl groups was performed using the modified Stöber method.[21] After 0.75 g of CTAB was dissolved in 20 mL of a 0.05 mol L^{-1} ammonia solution, 3.2 mL of ethanol was added to this reaction medium. The solution was stirred at 60 °C. Similarly, a mixture was prepared by mixing 1.49 mL of TEOS and 816 μL of PTES (30 mol-Si%), which was immediately transferred to the system containing the organic template, ethanol and ammonia. The solution was stirred for 120 min (starting from time $t = 0$) with two additions of 124 μL of TEOS at $t = 60$ min and $t = 90$ min to isolate the hydrophobic porous structure from the external environment. Next, nanoparticles were centrifuged and redispersed in ethanol to yield NP–CTAB–SiOH (raw nanoparticles containing CTAB). CTAB was extracted by transferring the nanoparticles to an ethanol/HCl (1 : 9) solution followed by 15 min of ultrasonication, centrifugation and resuspension in ethanol. The obtained nanoparticles are referred to as NP–SiOH (raw nanoparticles).

Functionalization of NP–CTAB–SiOH with silane PEG_{500} ($NP–10PEG_{500}$ and $NP–50PEG_{500}$)

The external surfaces of NP–CTAB–SiOH nanoparticles were functionalized with silane PEG_{500} according to previously reported procedures.[3,22] In this process, 300 mg of the raw nanoparticles containing CTAB were dispersed in 40 mL of absolute ethanol for 60 minutes, followed by homogenization for an additional 15 minutes at 60 °C. Then, silane PEG_{500} was added in an amount equal to 10% mol-Si related to the total number of moles of Si in TEOS and PTES from NP–SiOH. The reaction was performed under constant stirring at 60 °C for 1 hour, and the functionalization was continued for an additional 12 hours at room temperature. The products were subjected to centrifugation and redispersion in ethanol. CTAB was removed according to the experimental procedure described for the synthesis of NP–SiOH to obtain $NP–10PEG_{500}$.

This synthesis was repeated using silane PEG_{500} in an amount equivalent to 50% mol-Si based on the total number of moles of Si in TEOS and PTES (from NP–SiOH) to obtain $NP–50PEG_{500}$. The synthetic scheme of $NP–10PEG_{500}$ and $NP–50PEG_{500}$ is shown in Scheme 1(a).

Functionalization of NP–CTAB–SiOH with PEG_{2000} ($NP–10PEG_{2000}$)

Synthesis of $NP–10PEG_{2000}$ was performed according to functionalization procedures previously reported,[3,22] with 300 mg of NP–CTAB–SiOH dispersed in 62 mL of absolute ethanol for 30 minutes using ultrasonication. Then, silane GPS was added in an amount of 10% mol-Si related to the total number of moles of Si in TEOS and PTES from NP–SiOH followed by stirring for 12 hours at 85 °C in a nitrogen atmosphere. These experimental conditions are similar to the functionalization protocol reported by Liu *et al.*[23] Then, potassium hydroxide was added to the nanoparticles as a catalyst[24] to initiate the coupling reaction between the carboxylic function on PEG_{2000} and the glycidoxy group on the condensed silane GPS. Sequentially, PEG_{2000} was dissolved in ethanol by ultrasonication and then added to the flask containing the GPS-functionalized nanoparticles in the presence of KOH to initiate the coupling of mPEG–COOH (2000 Da). The reaction was maintained at 95 °C for 12 h according to the synthetic procedure reported by Liu *et al.*[23] CTAB was removed according to the experimental procedure described to obtain $NP–10PEG_{2000}$. The synthetic scheme of $NP–10PEG_{2000}$ is shown in Scheme 1(b).

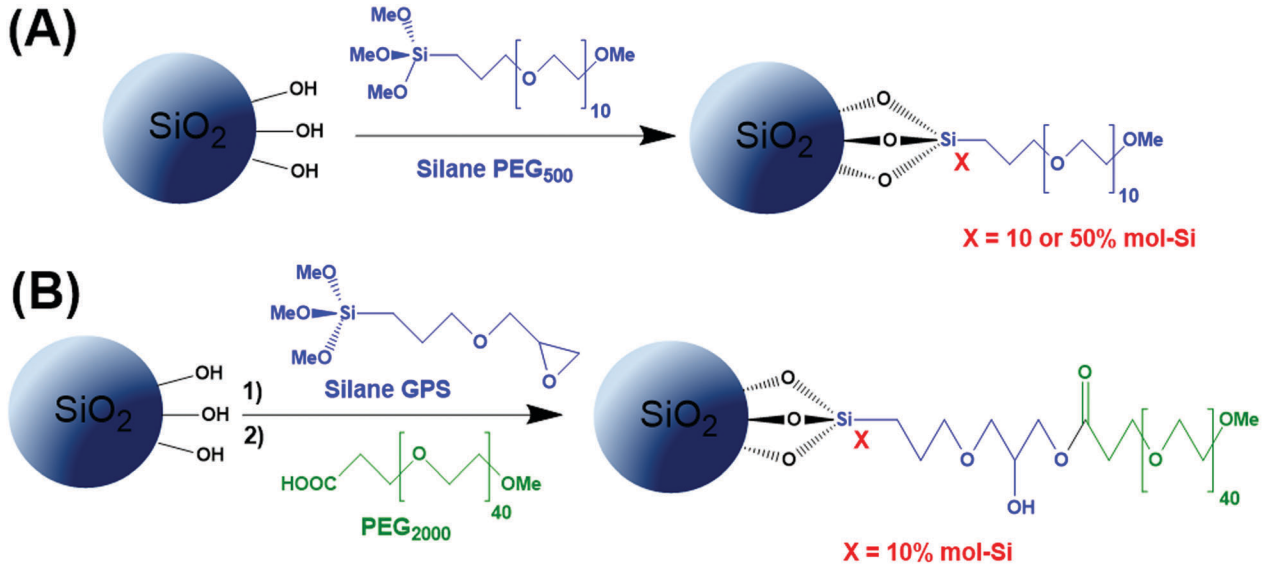

Scheme 1 Synthetic scheme of NP–10PEG$_{500}$, NP–50PEG$_{500}$ (A) e NP–10PEG$_{2000}$ (B).

Curcumin encapsulation

To each silica nanoparticle suspension (*i.e.*, NP–SiOH, NP–10PEG$_{500}$, NP–50PEG$_{500}$, and NP–10PEG$_{2000}$ (1 mg mL^{-1}, 10 mg)) was added 1 mg of curcumin. The nanoparticle + curcumin mixtures were subjected to ultrasonic homogenization for 30 minutes. Then, the systems were separated by decantation over 24 hours, and the supernatants were collected and subjected to UV-VIS spectroscopy to determine the curcumin concentration. To calculate the drug concentration in each sample, we constructed a calibration curve for curcumin in ethanol at five known concentrations (1, 5, 10, 30 and 50 μg mL^{-1}). For each concentration, the area under the absorption curve in the region between 200 and 550 nm was estimated to plot a graph of the area as a function of the concentration. Finally, to determine the concentration of encapsulated curcumin (mass of drug per unit volume), 1 mL of each suspension was subjected to UV-VIS spectroscopy, and the calculated area under the curve, which was estimated as described above, was compared with the calibration curve.

Characterization

^{29}Si nuclear magnetic resonance (NMR) spectra were recorded on a Bruker Avance 300 MHz using the HPDEC method (“high-power decoupling” → ^{29}Si ^{1}H). ^{13}C NMR spectra were obtained using the CPMAS method (“cross-polarization and magic angle spinning”); the speed rotation of the sample holder was 10 kHz for both silicon and carbon, under magic-angle spinning (54, 74°). Thermogravimetric analysis (TGA) was performed on a TA Instruments Thermal Analyzer 500, TGA module 2050. The morphology of the nanostructures was analyzed by transmission electron microscopy in bright-field mode (TEM, Zeiss Libra 120, operating at 80 kV). Dynamic light scattering (DLS) to evaluate the particle size and zeta potential (PZ) was carried out on a Malvern Zetasizer Nano-Instrument. Nitrogen sorption isotherms were obtained at 77 K in a Micromeritics ASAP 2020 analyzer. The surface area was calculated from the adsorption branch of the isotherm using the multipoint Brunauer–Emmett–Teller method (BET). Pore size distribution data and pore volume were calculated from the adsorption branch of the isotherm using the method of Barrett–Joyner–Halenda (BJH), and from the adsorbed quantity at a single point (P/P_0 = 0.94), respectively. The concentration of encapsulated curcumin in MSNs was estimated *via* light absorption analysis using an ultraviolet-visible spectrophotometer (Shimadzu model UV-1650 PC).

Results and discussion

Nanoparticle characterization

Mesoporous silica nanoparticles (MSNs) were firstly produced using a modified Stöber method that used phenyltriethoxysilane as a pore modifier for generating a hydrophobic microchemical environment in the inner pores, as well as for increasing the pore size.[25] Along with it, ethanol was used as the co-solvent, ammonia as a catalyst and cetyltrimethylammonium bromide (CTAB) as the template for generating mesopores. This modified Stöber method resulted in MSNs with high content of phenyl functions (30% mol-Si) within the pores. After the synthesis of MSNs, the nanoparticle outer surface was conjugated with PEG 500 and 2000 Da (molecular weights; see Scheme 1) prior to the template removal (see details in Experimental). The functionalization of the outer surface of the MSNs with PEG 500 Da (10 and 50% mol-Si) and PEG 2000 Da (10% mol-Si) was thoroughly assessed using multiple microscopic, spectroscopic and thermogravimetric analysis.

The thermogravimetric (TGA) and the differential thermal analysis (DTA) curves of the raw nanoparticles (NP–SiOH and NP–CTAB–SiOH) and functionalized nanoparticles (NP–10PEG$_{500}$, NP–50PEG$_{500}$ and NP–10PEG$_{2000}$) are shown in Fig. 1. The DTA data for NP–SiOH indicate a main event at 577 °C, related to the thermal decomposition of the phenyl groups. Because the final

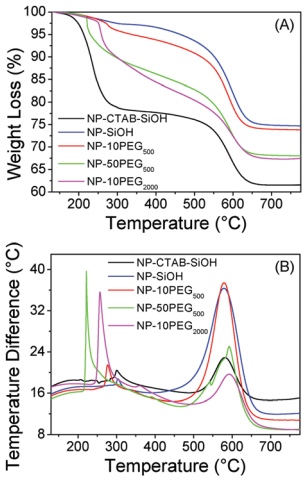

Fig. 1 TGA (A) and DTA (B) curves of the initial nanoparticles and pegylated nanoparticles.

sample was composed only of silica (SiO_2) with a mass of 74.6% at 900 °C, and phenyl groups with a calculated mass of 22.4% between 300 and 900 °C, we estimated experimentally that the number of Si bonded to these aromatic groups was of 23.4% mol-Si. For NP–CTAB–SiOH, which contains CTAB, the DTA data exhibited a significant event related to the decomposition of the organic template at 308 °C. The TGA curve of this molecular vehicle indicates that the decomposition of CTAB began at 135 °C and ended at 381 °C. The extraction of the surfactant from the pegylated nanoparticles was confirmed by the absence of its decomposition event on the corresponding curves in a temperature range between 135 °C and 381 °C.

For the nanoparticles functionalized with PEG_{500}, the TGA and DTA curves indicated an exothermic event between 210 °C and 470 °C due to polymer decomposition. The mass of polyethylene glycol in NP–10PEG$_{500}$ and NP–50PEG$_{500}$, calculated in relation to NP–SiOH, was of 0.9% and 6.8%, respectively, confirming its presence in increasing amounts in both nanoparticles. In the TGA and DTA curves of NP–10PEG$_{2000}$, a substantial exothermic event was observed in a temperature range between 230 °C and 500 °C, indicating the thermal decomposition of PEG_{2000} coupled to the GPS groups. The results indicate a mass difference of 6.9% between NP–SiOH and NP–10PEG$_{2000}$, which is consistent with a weight loss of polyethylene glycol.

Fig. 2A shows the ^{13}C NMR spectra, which were obtained using a method involving the cross-polarization of ^{1}H neighboring nuclei (CPMAS) in magic-angle spinning (MAS) mode, for the pegylated nanoparticles (ii–iv) and raw nanoparticles (i). For all nanoparticles, the carbon nuclei of the phenyl groups, numbered from 1 to 4 (note the chemical structure provided in Fig. 2), were observed in the region between 128.4 and 133.8 ppm. The presence of PEG_{500} was confirmed in the spectra of NP–10PEG$_{500}$ (ii) and NP–50PEG$_{500}$ (iii) *via* observation of its main nucleus (*i.e.*, carbon 5 at 72 ppm). The intensity of this peak in the NP–50PEG$_{500}$ spectrum was significantly higher compared to that for NP–10PEG$_{500}$, indicating a larger amount of functionalized silane PEG_{500} in the former. This information confirms the results of TGA and DTA analyses. The presence of PEG_{2000} was confirmed by the spectrum of NP–10PEG$_{2000}$ (iv), which showed peaks originating from carbon nuclei 5, 6 and 7 at 71.2 ppm, 60.1 ppm and 60.1 ppm, respectively.

The ^{13}C NMR results are consistent with thermal analysis, which confirmed the presence of PEG in all the functionalized nanoparticles. However, to evaluate the condensation of all silanes, ^{29}Si NMR spectra (Fig. 2B) were recorded using a high-power decoupling technique (HPDEC, $^{29}Si \rightarrow 1H$). In the

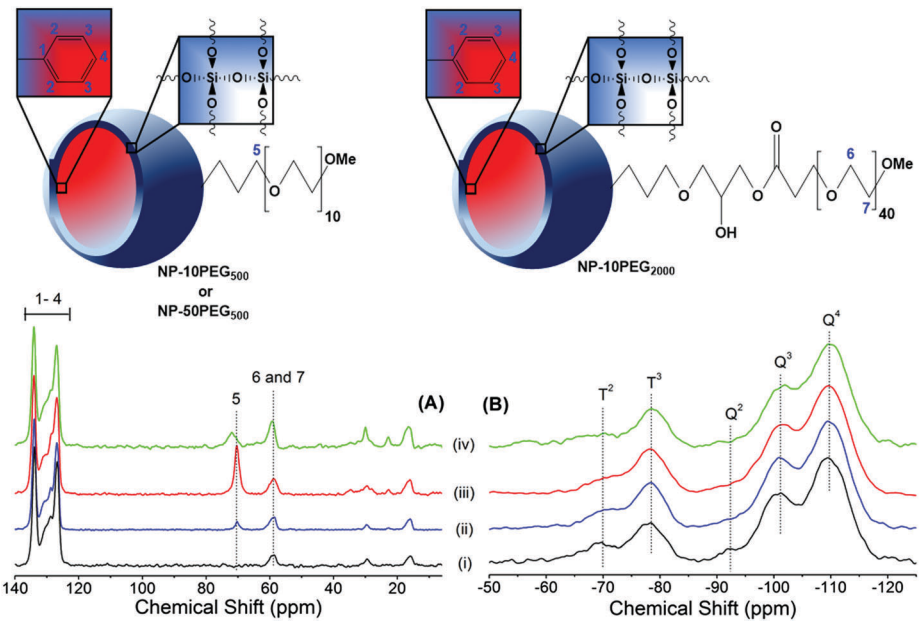

Fig. 2 ^{13}C NMR (A) and ^{29}Si NMR (B) spectra of NP–SiOH (i), NP–10PEG$_{500}$ (ii), NP–50PEG$_{500}$ (iii) and NP–10PEG$_{2000}$ (iv).

^{29}Si NMR spectra of all samples, peaks located at −110 ppm, −102 ppm, −93 ppm, −78 ppm and −70 ppm correspond to the Q^4, Q^3, Q^2, T^3 and T^2 silicon sites, respectively.[26] Analysis of the ^{29}Si NMR spectra of NP–10PEG$_{500}$, NP–50PEG$_{500}$ and NP–10PEG$_{2000}$ shown in Fig. 2B(ii–iv), after the PEG functionalization, revealed a decrease in the intensity of the Q^3 and Q^2 peaks (a reduction in the amount of structures HO–Si-(OEt)$_3$ and (OH)$_2$–Si-(OEt)$_2$, respectively) and an increase in the intensity of the T^3 and T^2 peaks (a larger amount of structures R–Si-(OEt)$_3$ and R–Si-(OEt)$_2$(OH), respectively), compared with those in the NP–SiOH spectrum (Fig. 2B). These results confirm the condensation of silanes PEG$_{500}$ and GPS onto the surfaces of the pegylated nanoparticles.

To complement these results and further analyse the surface features, nanoparticles were subjected to nitrogen adsorption–desorption analysis. Fig. 3A shows the results of the nitrogen adsorption–desorption analysis for all the studied nanoparticles. The nitrogen isotherm profiles are characteristic of type IV isotherms that are associated with mesoporous materials according to the IUPAC classification.[25,27] Furthermore, a typical hysteresis of a mesoporous material, characterized as the H3 type,[25,27] was observed for all samples. The hysteresis in this profile corresponded to a complex mesostructure. According to the pore distribution shown in Fig. 3B, which was calculated based on the BJH method, there is a predominance of pores between 4 and 10 nm in size, which is consistent with the nanoparticles exhibiting a mesoporous material profile. IUPAC classifies a mesoporous material as having a pore size distribution between 2 and 50 nm.[25,27]

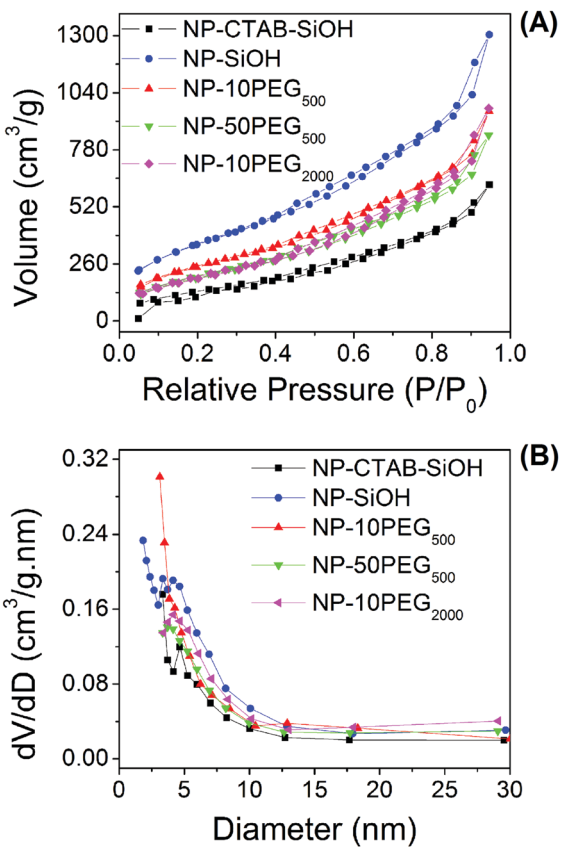

Fig. 3 Nitrogen adsorption–desorption isotherms (A) and pore size distribution (B) of the nanoparticles.

In addition to the nitrogen sorption experiments, the NP–SiOH and NP–50PEG$_{500}$ nanoparticles were analyzed using transmission electron microscopy (TEM); the TEM micrographs are shown in Fig. 4A and B, respectively. For both nanoparticles, the complex mesoporous structure was characterized by random porous cavities and pore sizes between 2 and 5 nm, generating an irregular topography and an average diameter of 65 nm. These results are in agreement with the results obtained from the N_2 physisorption technique. When available in large quantities (approximately 23% mol of the Si present in the MSN), the organosilane phenyltriethoxysilane increases the size of the micelles formed by CTAB, which generates porous cavities with larger sizes.

Table 1 lists the surface area, pore volume, particle size and zeta potential of the nanoparticles. The surface area and pore volume increased after the CTAB removal from NP–CTAB–SiOH to yield NP–SiOH, indicating an efficient removal of the organic template. According to the results, the pore volumes of NP–SiOH and NP–10PEG$_{500}$ were 2.2 cm^3 g^{-1} and 1.5 cm^3 g^{-1}, respectively, indicating that the presence of PEG in NP–10PEG$_{500}$ can sterically obstruct the adsorption of nitrogen. By increasing the functionalization rate to 50% mol-Si and increasing the polymer chain length, the pore volumes of NP–50PEG$_{500}$ and NP–10PEG$_{2000}$ did not change substantially in relation to that of NP–10PEG$_{500}$. Following the same reasoning, we can see that the decrease in the surface area was intrinsically related to the increasing functionalization rate and the increasing polymer chain weight (size). Interestingly, the increase in the functionalization rate led to a decrease in the MSN negative surface charges (*i.e.* zeta potential) because of the neutral characteristics of PEG, and a decrease in the amount of species SiO^- available on the outer surface of MSNs.

Curcumin encapsulation

Fig. 5 shows the calibration curve of curcumin in ethanol acquired at five known concentrations, and the graph of the curcumin concentration incorporated into the pegylated silica nanoparticles after decantation. According to the results, the straight line fitted with five points was suitable for estimating the curcumin concentration in a range between 1 and 50 μg mL^{-1}, once we have R^2 = 0.99.

First, the curcumin concentration in NP–10PEG$_{500}$ (5.4 ± 0.8 μg mL^{-1}) and NP–50PEG$_{500}$ (4.4 ± 0.7 μg mL^{-1}) was higher than the drug concentration in NP–SiOH (3.7 ± 0.2 μg mL^{-1}), indicating an increase in the encapsulation efficiency due to pegylation.

However, the amount of curcumin in NP–50PEG$_{500}$ is lower, which may be due to steric effects promoted by the higher PEG content on its outer surface. In addition, NP–10PEG$_{2000}$ (2.2 ± 0.2 μg mL^{-1}) encapsulated the smallest amount of curcumin compared to that encapsulated by the other nanoparticles. This result demonstrates a decrease in the drug encapsulation efficiency due to the higher weight of PEG$_{2000}$ compared to that

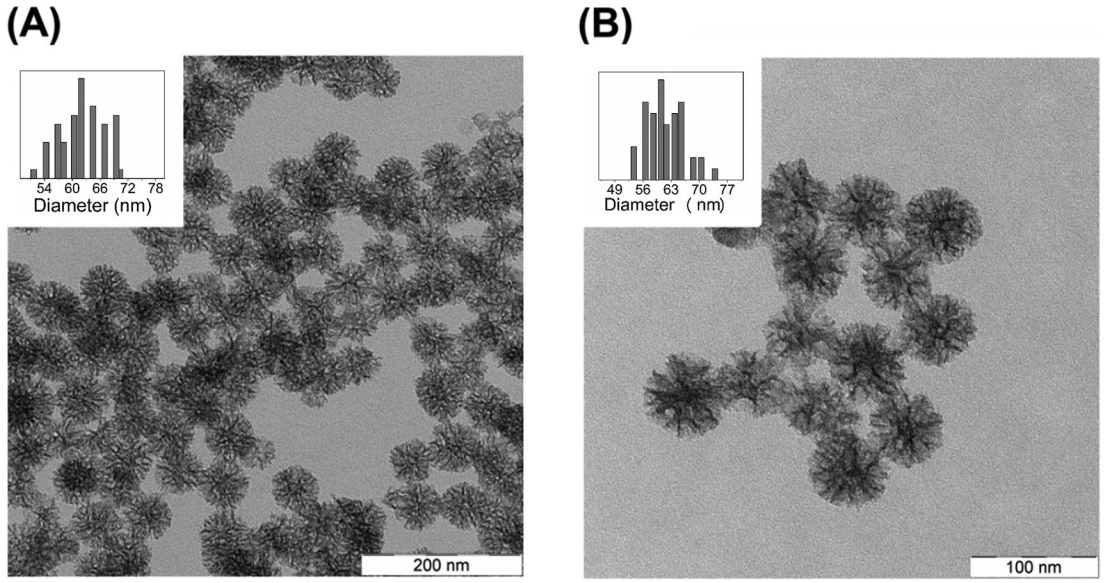

Fig. 4 Transmission electron microscopy (TEM) of NP–SiOH (A), NP–50PEG$_{500}$ (B) and their respective particle diameter distribution graphs.

Table 1 Surface area, pore volume, average size, PDI and zeta potential values of the nanoparticles

Sample	Surface area (m^2 g^{-1})	Pore volume (cm^3 g^{-1})	Average size (nm)	PDI	Zeta potential (ξ)	
					Value (mV)	STD (mV)
NP–CTAB–SiOH	548	1.0				
NP–SiOH	898	2.2	105	0.14	−20.5	5.8
NP–10PEG$_{500}$	943	1.5	116	0.24	−13.5	5.6
NP–50PEG$_{500}$	771	1.3	127	0.24	−8.8	5.4
NP–10PEG$_{2000}$	760	1.5	147	0.26	−6.0	4.7

of PEG$_{500}$, which indicates that the polymer size interferes on curcumin encapsulation. On the other hand, NP–10PEG$_{2000}$ exhibited the highest colloidal stability compared with those containing PEG$_{500}$.

Fig. 6 shows the NP–SiOH, NP–10PEG$_{500}$, NP–50PEG$_{500}$, and NP–10PEG$_{2000}$ suspensions encapsulated with curcumin, and the drug added to water (as a powder) in the absence of molecular vehicles (the image was taken after 24 hours of sedimentation). The hydrophobic characteristics of curcumin were evident in the clear supernatant in the flask containing H_2O. In the presence of silica nanoparticles, the yellow color of the supernatants, reflecting the presence of curcumin in the mesopores, also indicated the colloidal stability of the nanoparticles. Therefore, the results confirm the efficiency of pegylated MSNs to optimize the solubility of curcumin in water, making them suitable for intravenous applications. Furthermore, the presence

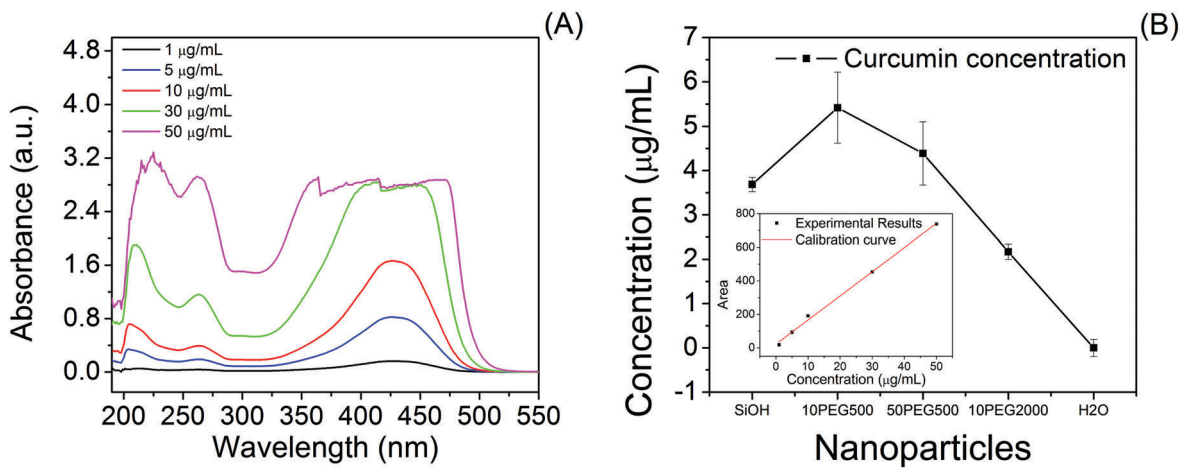

Fig. 5 Calibration curve for curcumin, its UV-VIS spectra (A) and concentration (B) of encapsulated curcumin in MSNs.

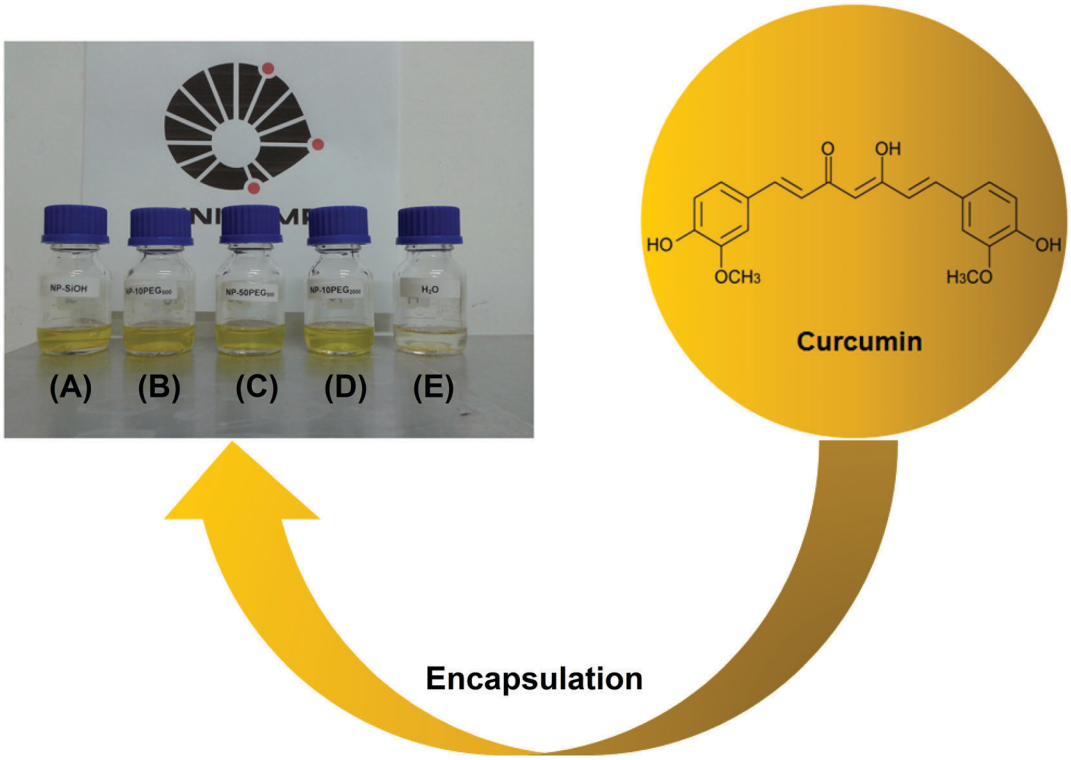

Fig. 6 The image of encapsulated curcumin inside the nanoparticles without PEG functionalization (A), pegylated nanoparticles NP–10PEG$_{500}$ (B), NP–50PEG$_{500}$ (C), NP–10PEG$_{2000}$ (D) and curcumin added to deionized water (E).

of PEG, besides providing a greater colloidal stability, it helps the drug to reach the target cells and avoids premature uptake by the immune system. On the other hand, the results for the encapsulation of curcumin reveal new issues that require further study to determine the optimal amount of functionalized polyethylene glycol and its influence on controlled drug delivery in biological applications. The highest colloidal stability was observed for the higher PEG weight (2000 Da). However, these nanoparticles contained the smallest amount of encapsulated drug. In future, the challenge of achieving high colloidal stability along with a suitable drug loading/release must be overcome.

The results of our study are important in the context of biological applications, such as antitumor treatment, because pegylation is essential for increasing the blood circulation time, preventing uptake by cells from the immune system, reducing specific interactions with RBCs to prevent hemolysis, as well as for providing low toxicity and greater biocompatibility. Additionally, the presence of hydrophobic functions, such as phenyl groups within the pores is crucial for the retention of hydrophobic drugs inside the nanoparticle to ensure that they reach the target cell during antitumor treatments, avoiding premature release and maintaining their physicochemical integrity.

Conclusions

Structural characterization using nuclear magnetic resonance confirmed the production of new pegylated silica nanoparticles. The results indicate that pegylated nanocarriers effectively improved the solubility of curcumin in water by increasing its concentration from approximately 0.6 μg mL^{-1} to 6.2 μg mL^{-1}, which overcomes the problem of water insolubility of the hydrophobic drug. In this context, the low solubility of curcumin in water is one of the problems addressed in this study, which demonstrated that pegylated MSNs are suitable nanocarriers for biomedical applications. We also observed that the amount of PEG and its size sterically influence the amount of encapsulated curcumin. Whereas PEGs with a high molecular weight increase the MSN colloidal stability and impair the curcumin loading in the nanoparticle pores. Finally, our findings show that the synthesized pegylated MSNs have potential as molecular carriers for curcumin in several biological applications. This advance was achieved by controlling the nanoparticle surface chemistry in the sol–gel method used.

Acknowledgements

We acknowledge financial support from CAPES, INCT-Inomat, Brazilian Nanotoxicology Network (Cigenanotox) and NanoBioss-SisNANO/MCTI.

Notes and references

1 H. Wu, G. Liu, S. Zhang, J. Shi, L. Zhang, Y. Chen, F. Chen and H. Chen, *J. Mater. Chem.*, 2011, **21**, 3037–3045.
2 H. Hu, H. Zhou, J. Du, Z. Wang, L. An, H. Yang, F. Li, H. Wu and S. Yang, *J. Mater. Chem.*, 2011, **21**, 6576–6583.

3 V. Cauda, A. Schlossbauer, J. Kecht, A. Zürner and T. Bein, *J. Am. Chem. Soc.*, 2009, **131**, 11361–11370.
4 C. Medina, M. J. Santos-Martinez, A. Radomski, O. I. Corrigan and M. W. Radomski, *Br. J. Pharmacol.*, 2007, **150**, 552–558.
5 H. Chen, C. Khemtong, X. Yang, X. Chang and J. Gao, *Drug Discovery Today*, 2011, **16**, 354–360.
6 J. E. Kipp, *Int. J. Pharm.*, 2004, **284**, 109–122.
7 V. P. Sant, D. Smith and J.-C. Leroux, *J. Controlled Release*, 2005, **104**, 289–300.
8 N. Yabuki, K. Sakata, T. Yamasaki, H. Terashima, T. Mio, Y. Miyazaki, T. Fujii and K. Kitada, *Cancer Genet. Cytogenet.*, 2007, **173**, 1–9.
9 K. Kato, K. Chin, T. Yoshikawa, K. Yamaguchi, Y. Tsuji, T. Esaki, K. Sakai, M. Kimura, T. Hamaguchi, Y. Shimada, Y. Matsumura and R. Ikeda, *Invest. New Drugs*, 2012, **30**, 1621–1627.
10 B. Joe, M. Vijaykumar and B. R. Lokesh, *Crit. Rev. Food Sci. Nutr.*, 2004, **44**, 97–111.
11 R. Wilken, M. S. Veena, M. B. Wang and E. S. Srivatsan, *Mol. Cancer*, 2011, **10**, 10–12.
12 M. W. Jeffrey and L. Xia, *CNS Neurol. Disord.: Drug Targets*, 2013, **12**, 487–497.
13 C.-Y. Lai, B. G. Trewyn, D. M. Jeftinija, K. Jeftinija, S. Xu, S. Jeftinija and V. S. Y. Lin, *J. Am. Chem. Soc.*, 2003, **125**, 4451–4459.
14 M. Liong, J. Lu, M. Kovochich, T. Xia, S. G. Ruehm, A. E. Nel, F. Tamanoi and J. I. Zink, *ACS Nano*, 2008, **2**, 889–896.
15 I. I. Slowing, J. L. Vivero-Escoto, C. W. Wu and V. S. Y. Lin, *Adv. Drug Delivery Rev.*, 2008, **60**, 1278–1288.
16 S. H. Wu, Y. Hung and C. Y. Mou, *Chem. Commun.*, 2011, **47**, 9972–9985.
17 Q. J. He and J. L. Shi, *J. Mater. Chem.*, 2011, **21**, 5845–5855.
18 D. R. Radu, C. Y. Lai, J. G. Huang, X. Shu and V. S. Y. Lin, *Chem. Commun.*, 2005, 1264–1266.
19 I. I. Slowing, B. G. Trewyn, S. Giri and V. S. Y. Lin, *Adv. Funct. Mater.*, 2007, **17**, 1225–1236.
20 J. L. Vivero-Escoto, I. I. Slowing, B. G. Trewyn and V. S. Y. Lin, *Small*, 2010, **6**, 1952–1967.
21 J. Kecht, A. Schlossbauer and T. Bein, *Chem. Mater.*, 2008, **20**, 7207–7214.
22 S. Huh, J. W. Wiench, J.-C. Yoo, M. Pruski and V. S. Y. Lin, *Chem. Mater.*, 2003, **15**, 4247–4256.
23 C.-H. Liu and C.-Y. Pan, *Polymer*, 2007, **48**, 3679–3685.
24 Y. Zhang, Y. Shen, D. Han, Z. Wang, J. Song and L. Niu, *J. Mater. Chem.*, 2006, **16**, 4592–4597.
25 A. J. Paula, L. A. Montoro, A. G. S. Filho and O. L. Alves, *Chem. Commun.*, 2012, **48**, 591–593.
26 A. van Blaaderen and A. Vrij, *J. Colloid Interface Sci.*, 1993, **156**, 1–18.
27 M. E. Hodson, *Geochim. Cosmochim. Acta*, 1998, **62**, 3429–3435.